Pergamon

Int. J. Solids Structures Vol. 32, No. 8/9, pp. 1285-1306, 1995

0020-7683/95 $9.50 + .00

0020-7683(94)00148-0

ELASTIC BUCKLING OF CYLINDRICAL SHELLS WITH ELASTIC CORES—II. EXPERIMENTS

G. N. KARAM and L. J. GIBSON
Department of Civil and Environmental Engineering, Massachusetts Institute of Technology, Cambridge, MA 02139, U.S.A.

Transmitted by John W. Hutchinson

(*Received* 14 *February* 1994; *in revised form* 10 *June* 1994)

Abstract—The analysis of the previous, companion paper showed that the buckling resistance of a cylindrical shell with a compliant core is greater than that of an equivalent weight shell without a core. Here, we describe uniaxial compression and four point bending tests on silicone rubber shells with and without compliant foam cores. The analysis describes the results of the mechanical tests well.

1. INTRODUCTION

In nature, thin cylindrical shells are often supported by a compliant elastic core. In the previous, companion paper (Karam and Gibson, 1994), we analysed elastic buckling of a thin walled cylindrical shell with a compliant core under uniaxial compression and bending. The analytical results indicated that such shells can be designed to have a higher buckling resistance than hollow shells of equal mass. The results were used to suggest that the elastic core in natural cylindrical shells gives rise to increased buckling resistance. In this paper we describe experiments which measure the elastic buckling response of silicone rubber shells with and without a compliant core under uniaxial compression and four point bending. The experimental results are well described by the analysis of the previous paper.

2. EXPERIMENTAL METHODS

To verify the predictions of the elastic buckling analysis of the previous paper, silicone rubber, a model linear elastic material, was selected for the experimental program. Silicone rubber cylindrical shells with and without compliant foam cores were tested in uniaxial compression and four point bending. The uniaxial compressive buckling strength was first measured on hollow cylindrical shells with no compliant core. The shells were then filled with a compliant core and re-tested. Each specimen was then cored to produce a central bore hole and re-tested; this procedure was then repeated for incrementally larger diameter bore holes. The local buckling strength in bending was measured on hollow cylinders and on cylinders partially filled with a compliant core. Typical uniaxial compression and four point bend specimens are shown in Fig. 1.

Uniaxial compression specimens

Silicone rubber cylindrical shells with nominal shell radius to wall thickness ratios a/t of 4.3, 10, 22, 31 and 48 were made. The two thickest shells ($a/t = 4.3$ and 10) were made by mixing liquid rubber (RTV 3110, Dow Corning Corporation, Midland, MI) with a slow acting catalyst, de-airing with a vacuum pump for 3–5 min, and pouring the mixture into concentric plexiglass molds for curing. The thinner shells ($a/t = 22$, 31 and 48) were made by mixing the liquid rubber with a fast acting catalyst, pouring it into a cylindrical mold and rotating the mold around its longitudinal axis at 500 rpm until curing was complete. This spin casting technique does not require de-airing as centrifugal force collapses all entrapped air bubbles and ensures nearly perfect thin walled cylinders. Each shell was 150

mm long. Three cylinders of each a/t ratio were made; the dimensions of each specimen are listed in Table A1 of the Appendix. Three tensile dogbone specimens were cast from each batch of silicone rubber for subsequent measurement of Young's modulus and Poisson's ratio.

The wall thickness of each cylinder was measured at three circumferential locations at each of two longitudinal positions using a spring loaded, weighted micrometer accurate to within 0.025 mm (Ames S-4325, B.C. Ames Co., Waltham, MA). Only cylinders with a coefficient of variation of wall thickness of less than 5% were used in subsequent mechanical tests. The mass of each cylinder was measured using an electronic balance (Sauter-E49, Ebingen, Germany), allowing the density of the silicone to be calculated.

After initial testing of the hollow shells in uniaxial compression, each shell was filled with a compliant core of foamed silicone rubber (RTV 3-6548, Dow Corning Corporation, Midland, MI) with a nominal relative density of 0.3. The rubber was foamed in place to ensure a good bond between the foam and the shell. The shells were supported in a split cylinder plexiglass mold during the foaming process to minimize distortions to the shell due to foam expansion. Four 20 mm cubes of foam, cut from blocks cast in the same batch, were used to determine its Young's modulus. Four rectangular strips 127 mm × 32 mm × 10 mm were used to determine Poisson's ratio of the foam. Foam densities were calculated from volume and weight measurements on four small rectangular block specimens (140 mm × 32 mm × 20 mm). The dimensions were measured with an electronic digital caliper (Max-Cal, Japan) and the weights measured on the Sauter-E49 balance. After testing the filled cylinders in uniaxial compression, a central cylinder of foam was removed using a hole saw in a drill press. The cylinder was then re-tested in uniaxial compression, the central bore hole diameter increased by some increment and the cylinder was re-tested. This procedure was repeated for bore hole diameters between 25 mm and 102 mm for each cylinder.

In addition, four pairs of hollow and partially filled cylinders of equal mass were made to compare their buckling resistance. The shells were made from silicone rubber while the cores were made of polyurethane foam. The core : shell modulus ratio was 0.013; the core depth was equal to ~ 1.6 half buckling wavelengths.

Four point bending specimens

Four point bending tests were performed on hollow silicone rubber cylinders and on silicone rubber cylinders partially filled with a compliant core. The cylindrical shells were spun in the same manner as uniaxial compression specimens using a larger mold operating at a higher speed (1200 rpm). The cylindrical shells had a length of 889 mm, an outside diameter of 146 mm and had radius to wall thickness ratios of $a/t = 17.6$, 22, 23, 32, 34, 40, 42 and 55. Two cylinders were made with $a/t = 23$ and $a/t = 32$; a single cylinder was made for each of the remaining a/t ratios. The wall thickness and a/t ratio of each of the cylinders are listed in Table A2 of the Appendix. Each cylinder was then cut longitudinally and bonded to a 25.4 mm thick flat sheet (889 mm long by 458 mm wide) of flexible polyurethane foam ($\rho = 15$ kg/m^3) using a thin layer of freshly mixed silicone rubber. The composite silicone rubber shell lined with the polyurethane foam sheet was then wrapped around a cylindrical mandrel, inserted into a split cylinder mold and bonded together along the seam line with more liquid silicone rubber to form a cylindrical shell with a compliant core. The thickness of the silicone rubber shells was measured in the same manner as the uniaxial compression shells while the shell was cut into a flat sheet. Measurements were made at 152 mm intervals across the sheet; only sheets with coefficients of variation of less than 10% were used in subsequent mechanical tests. The weight of the rubber used to bond the foam to the shell and to bond the longitudinal seam was measured by weighing the different components of the foam core cylinder as it was made. This weight was then added to the initial weight of the empty rubber tube and a corrected cylinder thickness calculated. Three 25.4 mm cubes of the flexible polyurethane were cut to determine its density and Young's modulus. Nine strips 152 mm × 25.4 mm × 13 mm were cut along each of three mutually perpendicular planes in the sheet to determine Poisson's ratio.

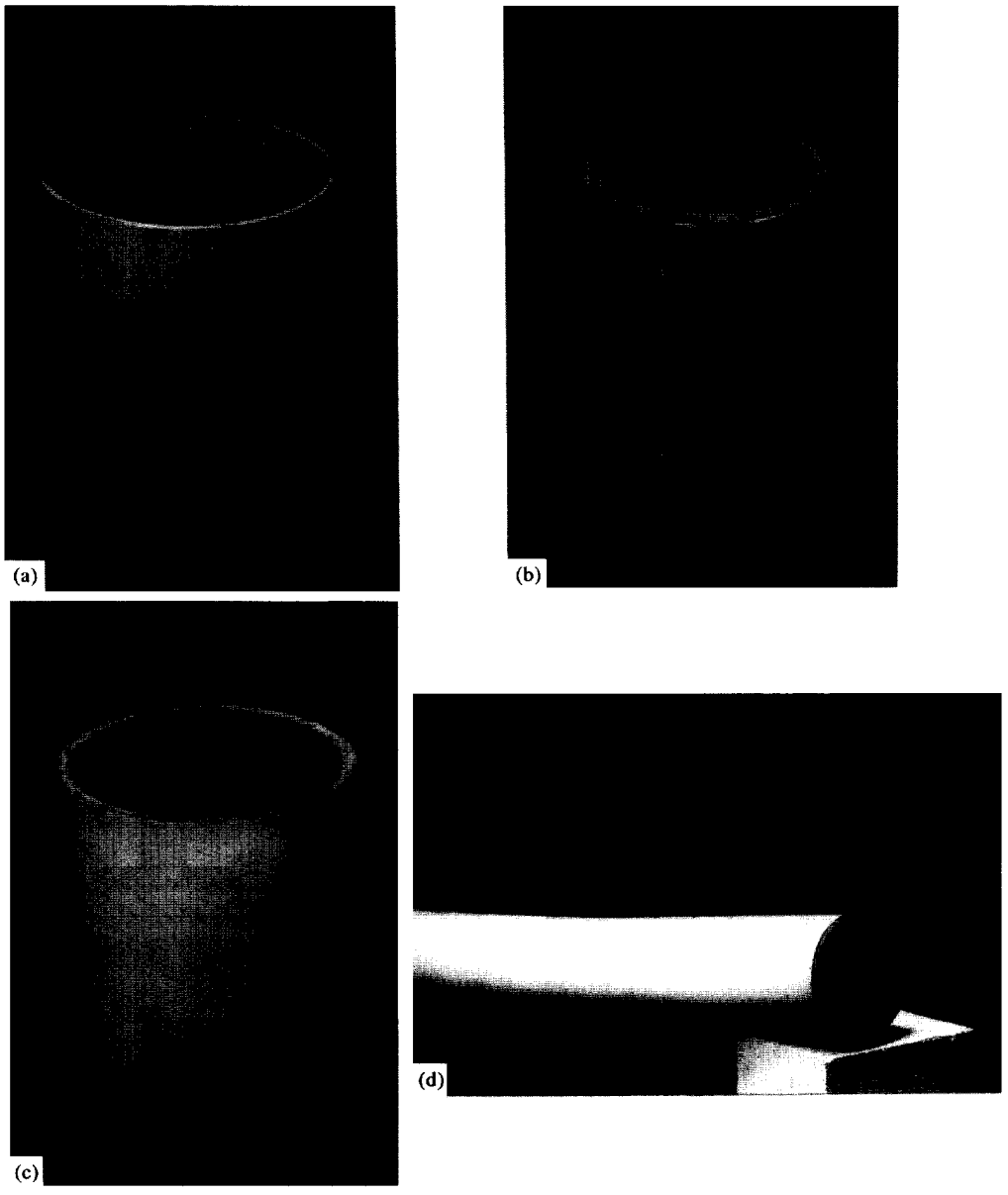

Fig. 1. (a) Hollow, (b) fully filled and (c) partially filled uniaxial compression specimens; (d) bending specimen.

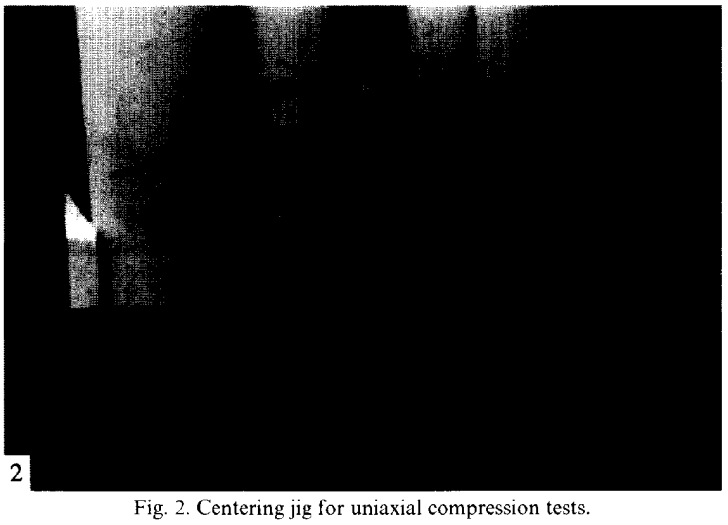

Fig. 2. Centering jig for uniaxial compression tests.

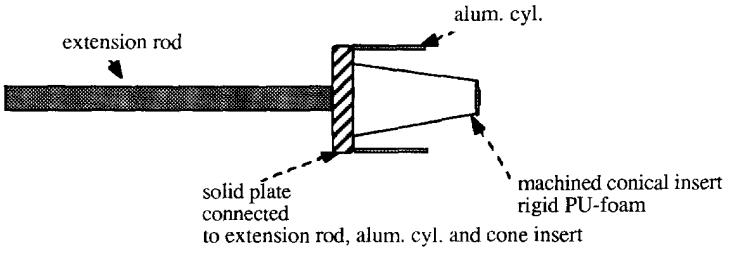

(a)

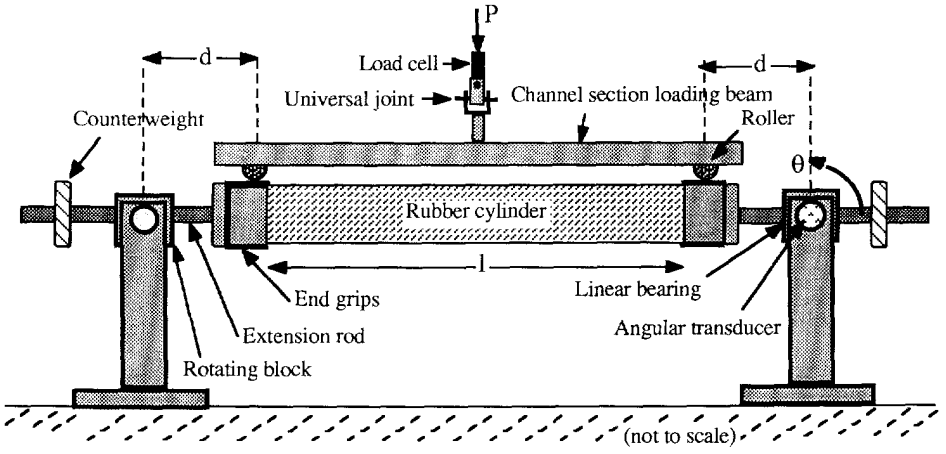

(b)

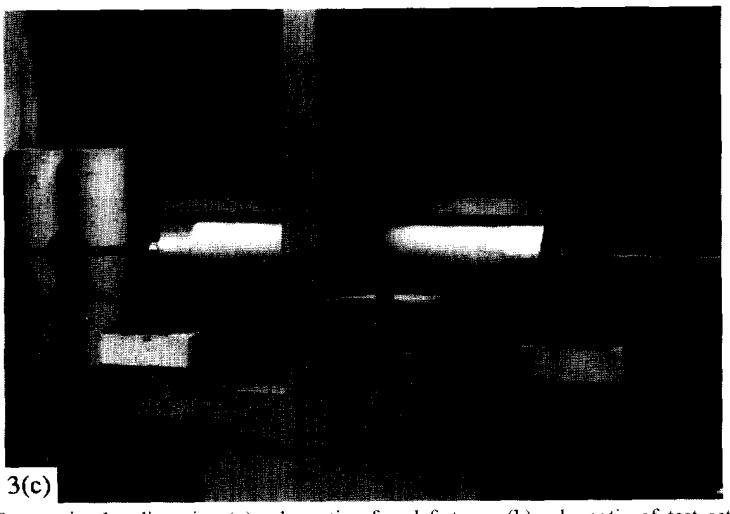

Fig. 3. Four point bending rig: (a) schematic of end fixture; (b) schematic of test set-up; (c) photograph of test set-up.

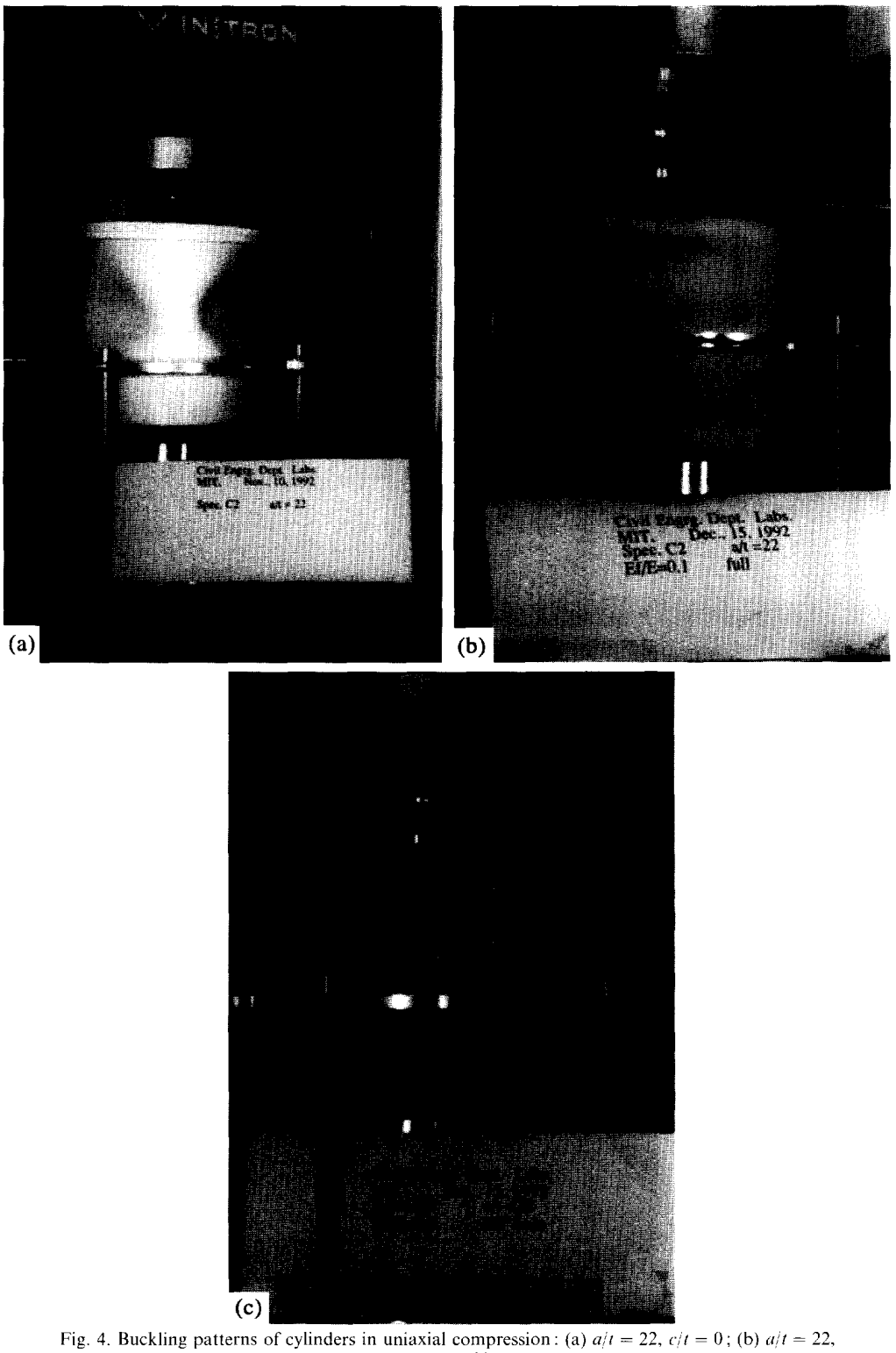

Fig. 4. Buckling patterns of cylinders in uniaxial compression: (a) $a/t = 22$, $c/t = 0$; (b) $a/t = 22$, $c/t = 21.5$; (c) $a/t = 22$, $c/t = 13.5$.

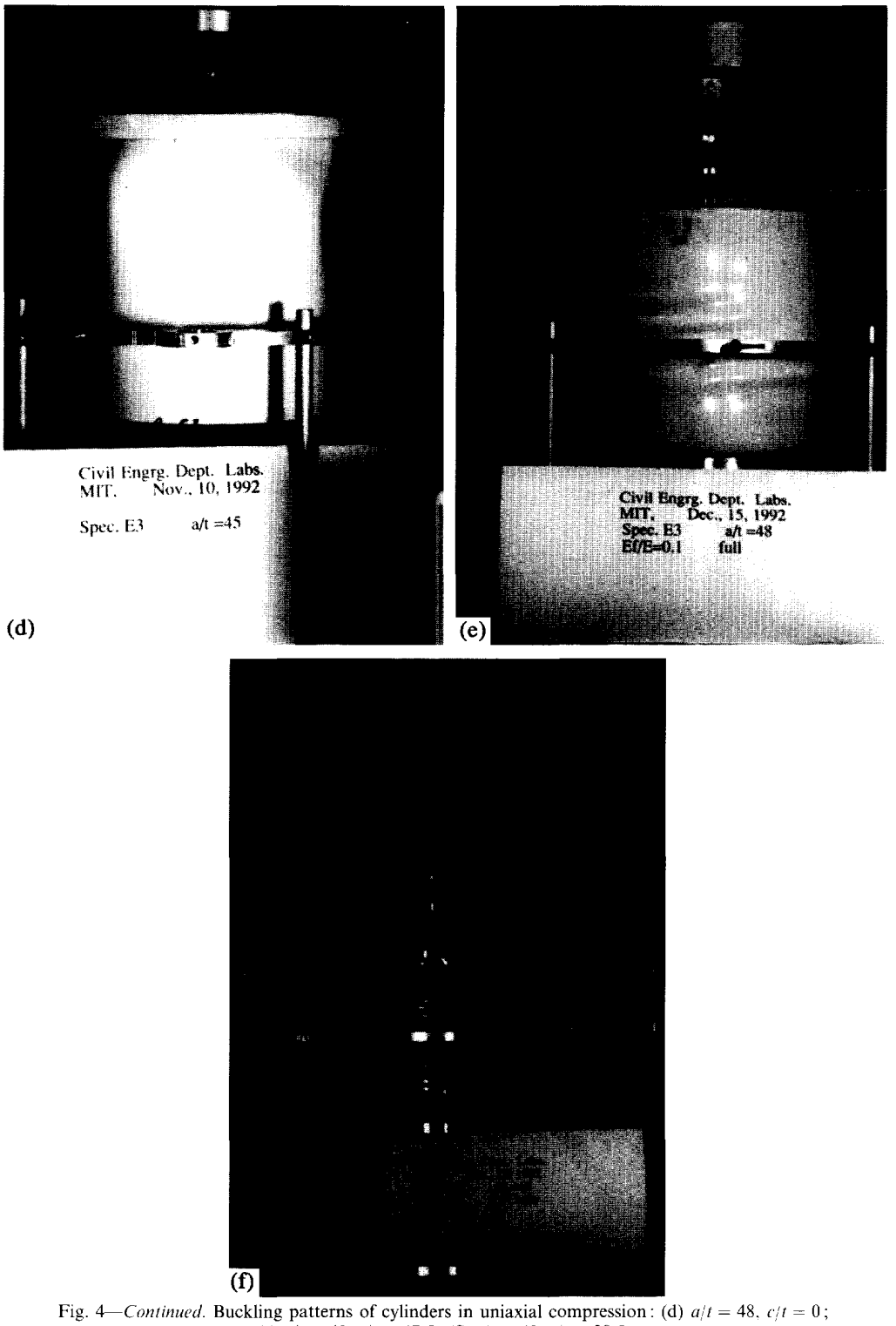

Fig. 4—*Continued.* Buckling patterns of cylinders in uniaxial compression: (d) $a/t = 48$, $c/t = 0$; (e) $a/t = 48$, $c/t = 47.5$; (f) $a/t = 48$, $c/t = 28.5$.

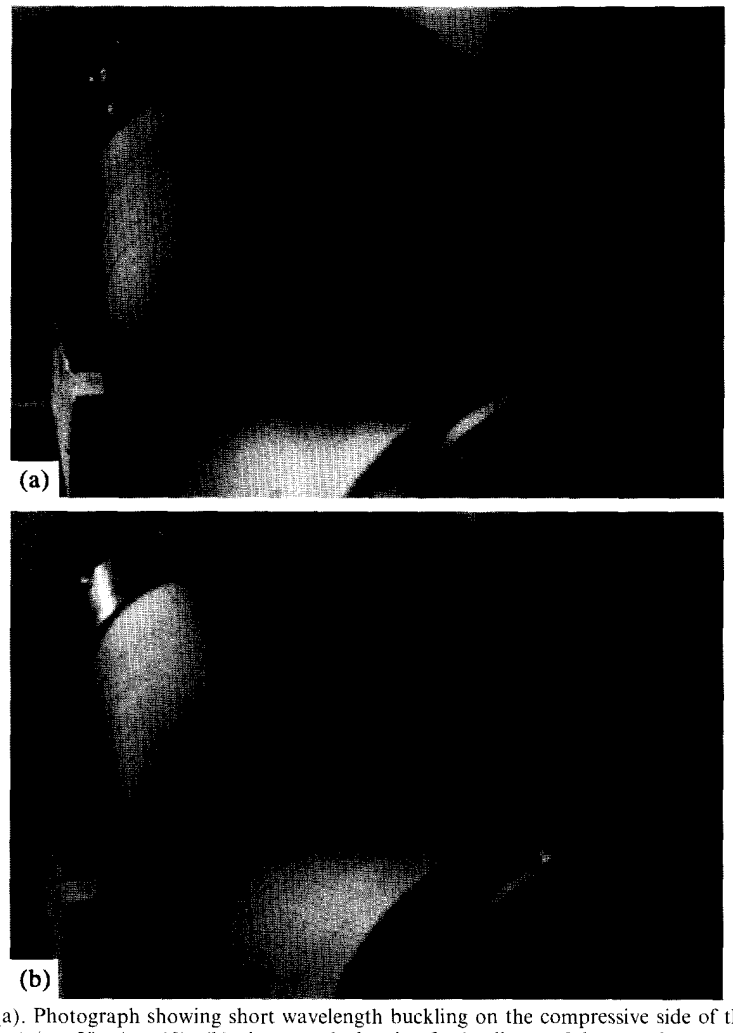

Fig. 11 (a). Photograph showing short wavelength buckling on the compressive side of the beam ($a/t = 28$, $c/t = 10$); (b) photograph showing final collapse of the same beam.

Mechanical tests

The Young's modulus and Poisson's ratio of the solid rubber was calculated from data from tensile tests on dogbone specimens using a universal testing machine (Instron Model 4201, Instron Corporation, Canton, MA). Three specimens from each batch were used to measure Young's modulus and one specimen from each batch was used to measure Poisson's ratio. One batch, from which a single cylindrical shell was made, was represented by only one dogbone specimen. The load was monitored through a 50 N load cell. The longitudinal and transverse displacements were monitored using a travelling optical microscope (Titan Tool Supply Co., Buffalo, NY) over 51 mm and 12.7 mm gage lengths, respectively; the gage lengths were marked by either steel pins or by a thin strip of rubber glued to the specimen. Both load and displacements were measured at increasing increments of crosshead displacement.

The Young's moduli of the silicone rubber and polyurethane foams were calculated from compression tests on cubic specimens using the same Instron testing machine. The load was measured with the 50 N cell and the displacement was taken as that of the crosshead. The Poisson's ratio of the silicone rubber foam was calculated from longitudinal and transverse elongations monitored with the travelling microscope over gage lengths of 38 mm and 28 mm, respectively, in tensile tests on thin strips. The Poisson's ratio of the polyurethane foam was measured in a similar fashion, with longitudinal and transverse gage lengths of 25mm, respectively.

The uniaxial compression tests on the cylindrical shells were also performed using the Instron Model 4201 testing machine. The hollow shells were tested first. The top and bottom edges of the shells were fitted into a grooved platen to maintain their circular cross-section at the ends. The top platen had two holes drilled into it to allow air inside the specimen to escape, preventing any internal pressure build-up. The specimens were centered along the loading axis of the machine using the special jig shown in Fig. 2. The load, applied through a steel ball centered to within 3mm, was recorded from the load cell while displacements were measured using the crosshead displacement transducer in the machine. The load–deflection data was obtained on an x–y plotter and recorded digitally by a data acquisition system (Hewlett-Packard HP 3497A, Data Control Unit) connected to a personal computer (Hyundai PC-XT). After buckling each test was stopped and the buckling pattern photographed.

On completion of the tests on empty cylinders, the specimens were filled with silicone rubber foam and re-tested using the same procedure. Central bore holes of increasing diameter were then made in the specimens. After each boring, the cylinders were again re-tested. Each buckling test was performed three times to verify the repeatability of the results.

While the axial compression tests followed an established and widely accepted procedure (Tennyson, 1963, 1964, 1967; Weingarten *et al.*, 1965a, b; de Neufville, 1965; Yamaki, 1984), there is no consensus on how to test thin walled tubes in bending. In order to study the moment–curvature relationship and buckling phenomena, a uniform bending moment has to be applied to all or part of the cylinder and maintained to relatively large deflections. Conventional four point bending is the simplest way to achieve a constant bending moment (Rhodes and Harvey, 1971), but at large deflections the loads transmitted through the vertical loading knives apply a drawing action on the rotated specimen (Cimpoeru and Murray, 1993) resulting in undesirable end restraints (Sherman, 1976). In the original work of Brazier (1927) and later Sherman (1983), a pure moment was applied at the ends of specimens rigidly attached to a rotating fixture; the prevention of axial movement of the fixtures caused unwanted axial tensile forces to develop at large deflections. McIvor *et al.* (1977) used a modified four point bending set-up that was suitable for large deflections but prevented the horizontal translation of the specimen, also leading to axial tensile forces. Reddy (1979) developed a modified four point test restraining the ends of the specimens by spring steel strips that allowed relatively large deflections and partial axial movement. Kyriakides and Shaw (1982, 1987) used a unique experimental rig that maintained constant force, direction and moment arm at large deflections while allowing some axial specimen movement. In their rig the specimen ends are inserted into two wheels each carrying two

points of a four point loading set-up. The wheels are rotated in opposite directions by shortening a chain running around them, applying a uniform bending moment to the tube in between the wheels. More recently, Cimpoeru and Murray (1993) have used a variation on this set-up. Given the requirements of our experimental program (large beam curvatures, free rotation at the supports, free axial movement, special grips to transmit loading to the beams), we have found it necessary to design and build a modified four point testing rig that can be used with conventional testing machines and yet provide the required characteristics.

The specially built loading rig, designed to be used in the Instron testing machine, is shown in Fig. 3. The specimens were gripped at the ends with a closely fitting external cylinder and a tapered conical insert. Each specimen had two 3 mm diameter holes drilled into it near the end grips to allow air inside the specimen to escape, preventing any internal pressure build-up. The end grips were extended by solid hardened steel rods fitted into linear bearings, allowing free axial movement in and out of the block supports. Each block support rested on two rotational bearings allowing free rotation in the plane of loading. The load was applied through a universal joint at the midpoint of a loading beam with rollers at fixed locations at its ends. The self-equilibrating loading beam splits the load applied by the machine into two equal forces applied to the end grips at a constant horizontal distance d from the center of the support blocks. Sliding counterweights were fitted to the steel rods extending beyond the supports allowing an initial constant moment to be applied to the specimen if needed.

The load was measured using a 500 N load cell while the curvature of the beams was monitored with an angular displacement transducer (Model 0605, Transtek Inc., Ellington, CT) measuring the rotation at the supports (Fig. 3). The load cell and rotation transducer were both connected to the computerized data acquisition system described above. The bending stiffness of the grips and extension rods was designed to be much larger (about 2.5×10^3) than that of the specimens tested so as to concentrate all deformation in the free spanning part of the cylinder. By adjusting the free span of the cylinder l and the moment arm d (Fig. 3) in the loading set-up, the magnitude of the moments and curvatures applied can be widely varied while keeping the support rotations small and the loading geometry constant. For small end rotations, $\theta \leqslant 15^\circ$, the curvature of the cylinder C and the moment M, due to the applied load, are given by

$$C = \frac{2\theta}{l}$$

$$M = \frac{Pd}{2} \tag{1}$$

where θ is in radians.

Under their self weight, the cylinders deflect, rotating the ends. This initial end rotation was then reduced to zero by setting the counterweights appropriately. At the beginning of the test, the cylinder was in a fixed–fixed end condition with zero rotation and curvature at the supports. At this point, the cylinder was subject to its own dead weight between the grips and the end moment from the counterweights causing an initial moment M_{dl} and curvature C_{dl} at the midspan of the beam. The cylinders were then loaded to failure using the Instron Model 4201 with a crosshead speed of 5 mm/min. Under these conditions the cylinders buckled locally in the middle away from the end grips. Failure was defined as the loss of moment carrying capacity.

In a separate series of tests, the ovalization of the midspan of the beams was measured with the travelling microscope for fixed bending moments applied by the counterweights. The rotation at the support was measured with the angular rotation transducer.

3. EXPERIMENTAL RESULTS

The measured density, Young's modulus and Poisson's ratio of the solid silicone rubber, foamed silicone rubber and foamed polyurethane used in the experimental program

Table 1. Material properties

Property	Solid rubber	Foam rubber	Foam polyurethane
Density (Mg/m^3)	1.17 (0.022)†	0.40 (0.01)	0.015 (0.002)
Young's modulus (MPa)	2.2‡	0.20 (0.024)	0.028 (0.0032)
Poisson's ratio (−)	0.48 (0.009)	0.32 (0.073)	0.45 (0.10)§

† The number in parentheses is the standard deviation.

‡ Values for the Young's modulus varied between 1.41 and 2.39 GPa, depending on the type of catalyst and the amount of thinner used. The theoretical buckling loads and local bending moments were calculated using the value of E corresponding to the batch from which each cylinder was made (see Tables A1 and A2).

§ The polyurethane foam was anisotropic with Poisson's ratios averaging 0.3, 0.46 and 0.55 along three orthogonal axes. In the numerical model, ν_c was set to 0.3. Both 0.3 and 0.45 give negligible ovalizations, and the use of 0.45 instead of 0.3 for the local buckling stress results in an overestimate of the buckling stress of less than 5%.

are listed in Table 1. The solid and foamed silicone rubber showed linear elastic stress–strain relationships within the tested range, up to 25% strain. The foamed polyurethane showed linear elastic behavior up to 12% compressive strain. The ratio of the core to shell moduli for the rubber foam is $E_c/E \approx 0.1$, while for the polyurethane foam it is $E_c/E \approx 0.01$.

Under uniaxial compression, the hollow cylinders buckled in a diamond pattern showing buckling wavelengths in both the circumferential and longitudinal directions, while the cylinders with the compliant core buckled in the axisymmetric mode with only longitudinal wavelength (Fig. 4). The longitudinal buckling wavelength of the hollow cylinders was, as expected, several times that of the foam core cylinders. For a given cylinder with a compliant core, increasing the bore hole diameter had little effect on the buckling wavelength until the core became very thin (core to shell ratio c/t of about 5). At this point the shell and underlying foam acted as an equivalent isotropic shell and buckled together as a unit. Typical load–deflection curves for three hollow cylinders are shown in Fig. 5. The normalized uniaxial buckling stress σ_{cr}/E for the hollow cylinders is plotted against the ratio of shell radius to wall thickness a/t in Fig. 6. Each point represents the average buckling load of tests on three cylinders; the vertical lines represent the maximum and minimum buckling loads. The buckling load for each cylinder was obtained by averaging three repeated buckling measurements; the variation in single cylinder measurements did not exceed 5%. The calculated buckling load, given by eqn (1) in the companion paper, is represented by the solid line in the figure; the theory describes the data well. The load–deflection curves for the fully and partially filled cylinders show several distinct behaviours (Fig. 7). In the thicker walled cylinders ($a/t = 4.3$, 10) buckling causes a decrease in load; if the core is sufficiently deep, it can carry additional load at reduced stiffness after buckling of the shell [Fig. 7(a)]. This behavior is consistent with the numerical predictions of Almroth and Brush (1963) for the postbuckling behavior of core stabilised cylinders. At $a/t = 22$, there is a transition in behaviour; cylinders with thick cores show bilinear behaviour with

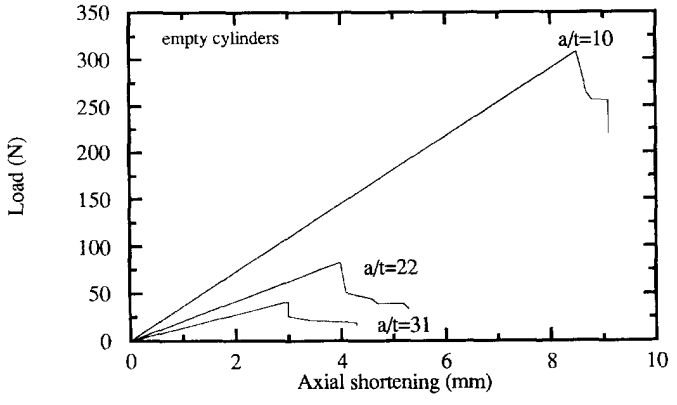

Fig. 5. Load–axial shortening curves for hollow cylinders in uniaxial compression.

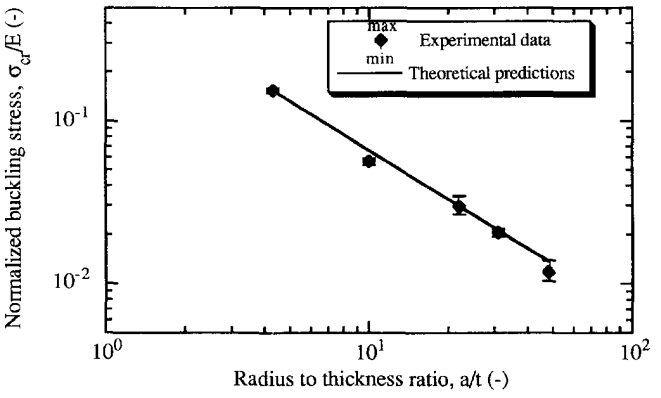

Fig. 6. Normalized buckling stress σ_{cr}/E plotted against radius to wall thickness ratio a/t for hollow cylinders loaded in axial compression.

reduced slope at higher loads while the cylinders with thin cores show a maximum load at which buckling occurs [Fig. 7(b)]. Furthermore, the thinnest walled cylinders ($a/t = 31, 48$) all show a bilinear load–deflection curve [Fig. 7(c)]. Axisymmetric buckling was observed to occur at the peak load in curves with a maximum or at the point at which the slope of the load–deflection curve reduced in the bilinear curves. Data for the uniaxial buckling loads are plotted against the core to thickness ratio c/t in Fig. 8. The measured buckling loads are normalized by the theoretical buckling load for the hollow cylinder of the same a/t. Each point represents the average buckling load of tests on three cylinders; the vertical lines represent the maximum and minimum buckling loads. The leftmost point on each plot represents the hollow cylinder ($c/t = 0$), while the rightmost point represents the fully filled cylinder ($c/t = a/t - 1/2$). Intermediate points at increasing c/t correspond to increasing core thickness. The value of c/t for which the stresses within the core theoretically decay to a negligible level is indicated by $(c/t)_0$.

In Fig. 9, the number of axisymmetric buckling wavelengths for the fully filled tubes is plotted against the radius to shell thickness ratio a/t. The solid line represents the number of wavelengths calculated based on the initial length of the cylinder, while the dashed line represents that based on the actual shortened length of the cylinder at the instant of buckling. Figure 10 shows the uniaxial buckling stress for the fully filled cylinder of given a/t divided by the buckling stress of a hollow cylinder of same a/t, σ_{cr}/σ_0, plotted against the dimensionless core stiffening parameter suggested by Seide (1962), $(a/t)^{3/2}(E_c/E)$, comparing our results with theoretical predictions and a compilation of data from the literature.

Four pairs of hollow and partially filled cylinders of equal mass were tested in uniaxial compression to compare their buckling resistance. The cores of the partially filled cylinders were made of polyurethane foam with a core : shell modulus ratio of 0.013; the core depth was equal to 1.6 buckling half wavelengths. The buckling loads are compared in Table 2. The partially filled cylinders had measured buckling loads ranging from 1.35–3.70 times those of the hollow cylinders of equal weight, in comparison to theoretical buckling load ratios of 1.8–5.22.

The results of the four point bend tests are shown in Figs 11–15. Figure 11 shows photographs of local buckling of the compressive face and final collapse of a partially filled cylinder. Figure 12 shows moment–curvature relationships for typical hollow and partially filled cylinders. The two measurements shown on each graph are made with the seam of the tube at the neutral axis rotated either plus or minus 180°; the local buckling moment was taken to be the maximum moment capacity of the beam and was calculated from the average of the two measurements. The initial offset arises from the initial dead load, as described in the methods section. The average local buckling moment for the hollow cylinders is plotted against the shell radius to wall thickness ratio a/t in Fig. 13(a). The degree of ovalization of one of the hollow cylinders is plotted against curvature in Fig. 13(b). The degree of ovalization of the partially filled cylinders was measured to be less

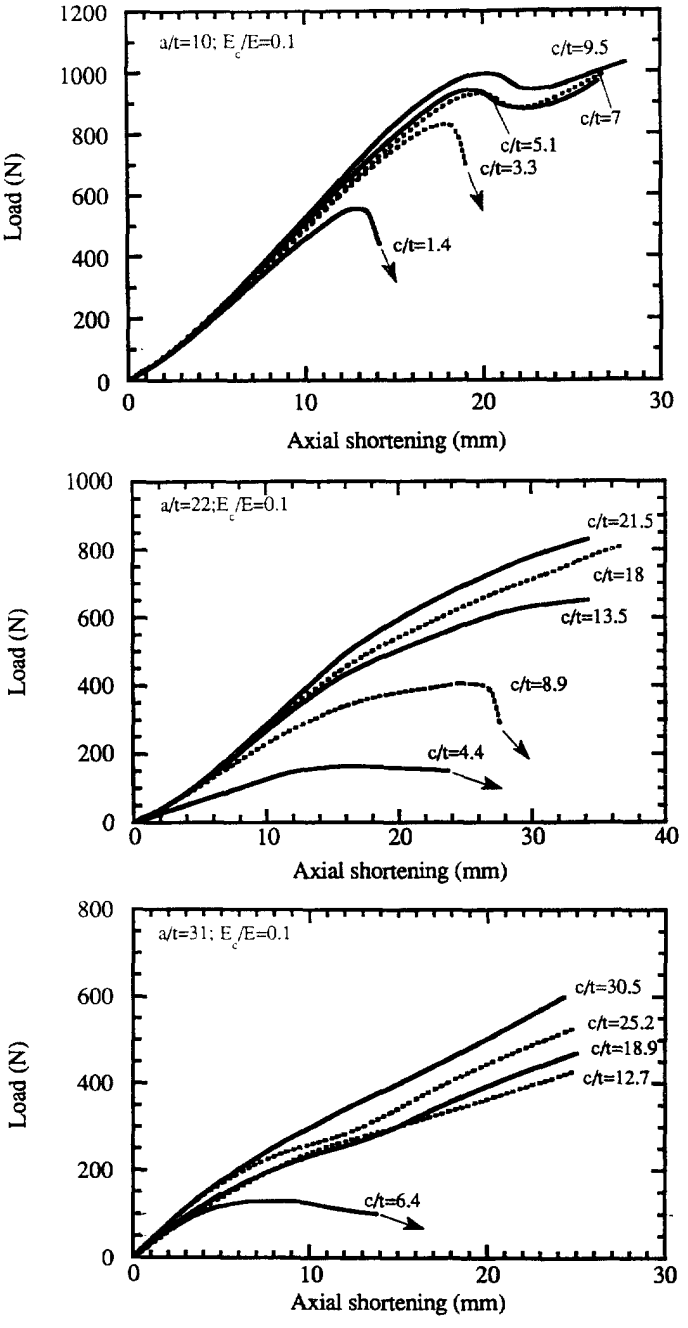

Fig. 7. Load–axial shortening curves for foam filled cylinders: (a) $a/t = 10$; (b) $a/t = 22$; (c) $a/t = 31$.

than 1.5% for curvatures up to 0.6 m^{-1}, which we took to be negligible. The average local buckling moment of the partially filled cylinders is plotted against the shell radius to wall thickness ratio a/t in Fig. 14. Figure 15 plots the ratio of the measured local buckling moments of the partially filled cylinders to the theoretical local buckling moment of hollow cylinders of equal weight. Superimposed on the figure are the ratios predicted from the analysis of the companion paper [eqn (35)]. Table 3 compares the theoretical and experimental local buckling moments of four pairs of partially filled and hollow cylinders of equal weight. The partially filled cylinders had measured buckling moments ranging from 2.43–4.84 times those of the hollow cylinders of equal weight, in comparison to theoretical buckling load ratios of 2.15–2.99.

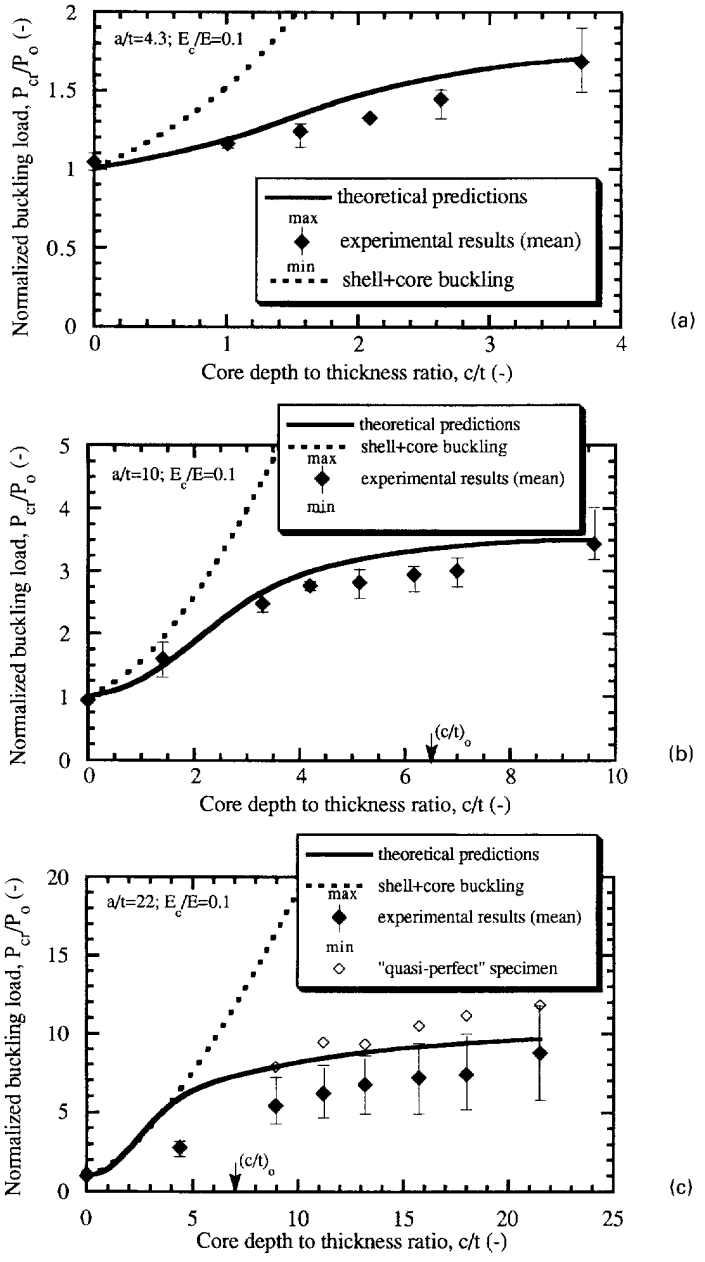

Fig. 8. Measured buckling load in uniaxial compression normalized by the theoretical buckling load of a hollow cylinder of the same a/t plotted against the core to shell thickness c/t: (a) $a/t = 4.3$; (b) $a/t = 10$; (c) $a/t = 22$.

4. DISCUSSION

Uniaxial compression

The load–deflection curves for the hollow cylinders in uniaxial compression show a well-defined maximum load at which buckling occurs (Fig. 5). The measured buckling loads are described well by the analysis of the previous, companion paper [eqn (1)] (Fig. 6). The excellent agreement between the analysis and data is due to the near perfection of the specimens produced by the spin-casting manufacturing technique (Tennyson, 1963, 1967) and to the relatively small radius to thickness ratios used.

Data for the effect of increasing the central bore hole diameter on the uniaxial buckling load are compared with the analysis in Fig. 8. The solid line represents the calculated normalized buckling load, using eqns (1), (10) and (30) of the companion paper. For values

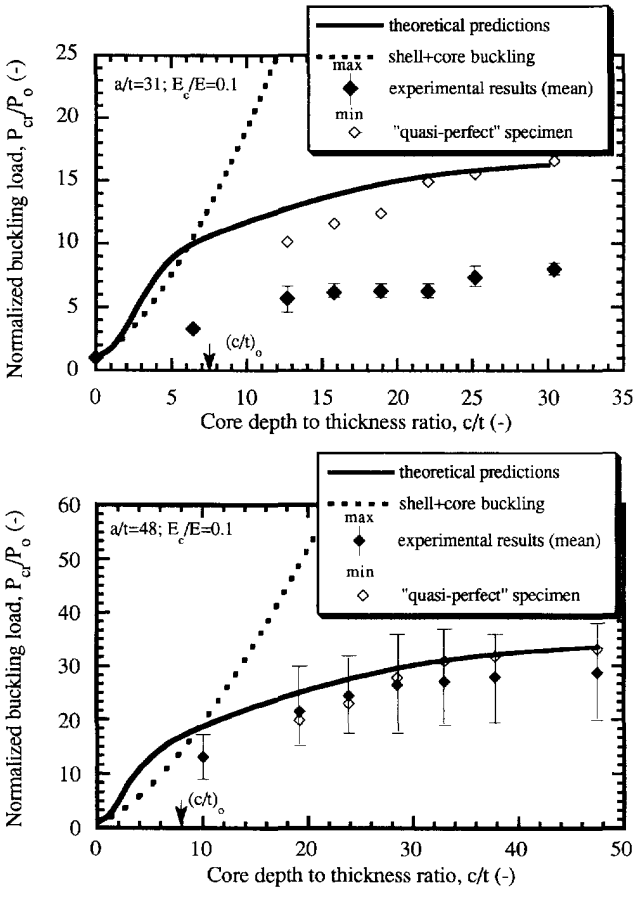

Fig. 8—*Continued.* Measured buckling load in uniaxial compression normalized by the theoretical buckling load of a hollow cylinder of the same a/t plotted against the core to shell thickness c/t: (d) $a/t = 31$; (e) $a/t = 48$.

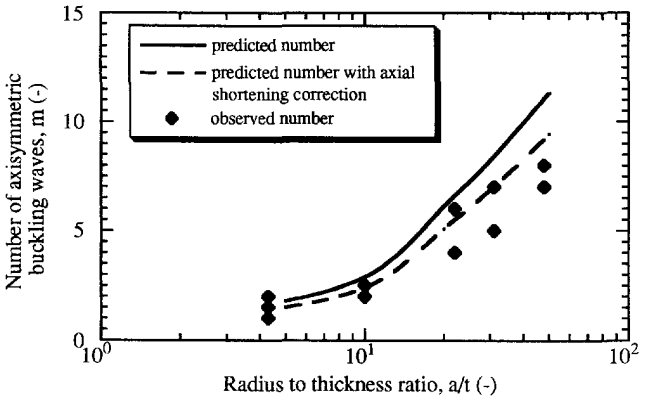

Fig. 9. Number of axisymmetric buckling wavelengths for foam filled cylinders in axial compression plotted against radius to shell thickness ratio a/t.

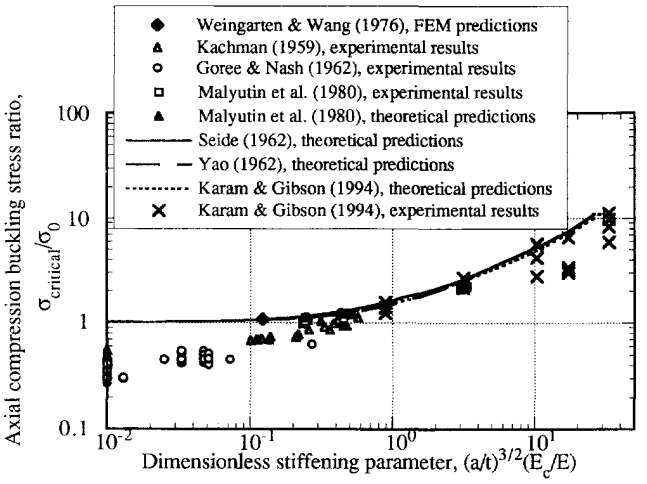

Fig. 10. Uniaxial buckling stress ratio plotted against Seide's dimensionless stiffening parameter.

Table 2. Uniaxial compression buckling loads for hollow and partially filled cylinders of equal weight

Mass (g)	a/t	c/t	P_{expt} (N)	P_{theory} (N)	$P_{core}/P_{empty}(-)$ (experiment)	$P_{core}/P_{empty}(-)$ (theory)
228	32.5	12.5	160	166	1.54	1.80
218	22	—	104	92		
157	40	15	73	108	1.35	2.00
150	26	—	54	54		
671	65	11	290	400	2.44	3.01
710	37	—	119	133		
352	125	21	85	235	3.70	5.22
350	65	—	23	45		

Cylinders had solid silicone rubber shells with a flexible polyurethane core with $c/t \approx 1.6$ buckling half wavelengths.

of $c/t < (c/t)_0$ (that is, core thicknesses less than that required for the stresses in the core to decay to a negligible value), the modulus of the elastic foundation k_e was modified as follows (Gough *et al.*, 1940):

$$k_e = \frac{2E_c}{\lambda} \frac{\sinh\left(\frac{c}{\lambda}\right)\cosh\left(\frac{c}{\lambda}\right) - \frac{c}{\lambda}}{(3-\nu_c)(1+\nu_c)\sinh^2\left(\frac{c}{\lambda}\right) + (1+\nu_c)^2\left(\frac{c}{\lambda}\right)^2 + 4} \tag{2}$$

where the variables are defined in the previous paper. The dashed lines describe combined buckling of the shell and core [eqn (29) of the previous paper]. The mean buckling load is indicated by the filled diamond points with a vertical line representing the range. The theory describes the data well for $a/t = 4.3$ and 10, confirming the use of the analysis for stress decay within the core. For $a/t = 22$ and 48, the mean measured buckling loads are about 75% of that expected, and for $a/t = 31$, they are about 50% of that expected. The discrepancies arise from imperfections in the thinner walled shells and, at very low c/t, from accumulated damage from repeated coring and testing. Imperfections arose from internal pressure in the core during the foaming process causing barrelling of the thinner shells such that an originally straight longitudinal strip of the shell bowed out slightly. Profile measurements of the thicker walled shells ($a/t = 4.3$ and 10) showed negligible barrelling with maximum amplitudes of between 1 and 2 mm, corresponding to one tenth to one third of the shell thicknesses. Some of the thinner walled shells ($a/t = 22$, 31 and 48), on the other hand, gave an approximately sinusoidal profile with a maximum amplitude varying between 3 and 5 mm, or one to three times the shell thickness. The profiles fit the equation

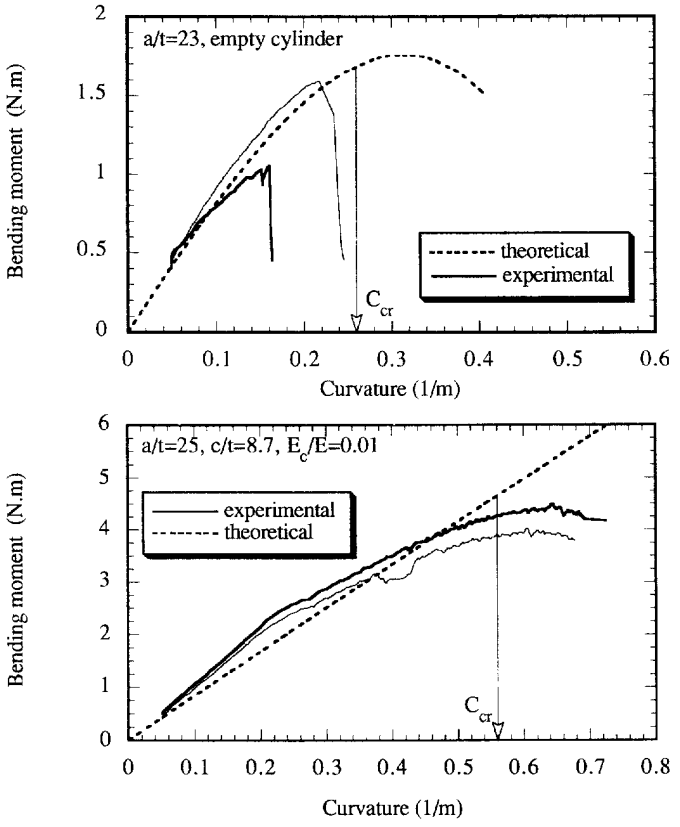

Fig. 12. Moment–curvature curves for cylinders in four point bending. The theoretical critical curvature at which local buckling initiates is indicated by the arrow: (a) hollow cylinder; $a/t = 23$; (b) partially filled cylinder, $a/t = 25$, $c/t = 8.7$.

$z = z_{max} \sin(\pi x/150)$ with a correlation factor $R > 0.92$, where z is the outward displacement, z_{max} is the maximum barrelling amplitude in mm given in the Appendix (Table A3), x is the distance in mm along the length and z and x are measured in mm. Given the long wavelength of the imperfection, it seems that the decrease in the buckling load is dependent on the maximum amplitude of the barrelling. For the profiles measured, specimens D4 ($a/t = 31$), D5 ($a/t = 31$) and E2 ($a/t = 48$) showed the most barrelling and the corresponding highest reduction in the buckling stress.

Previous investigations indicated that, for an axisymmetric imperfection in the shape of the buckling mode of amplitude equal to the thickness of the shell, the buckling load of a hollow shell is reduced by 75% (Koiter, 1963). The presence of relatively small internal pressures can reduce the drop in the buckling loads to less than 30% (Hutchinson, 1965 a, b); the effect of the compliant core in our specimens is similar to that of internal pressure, reducing the effect of initial imperfections.

To verify that barrelling was the correct cause of the discrepancy between measured and theoretical buckling loads, three additional cylinders, made so as to reduce the bowing, were tested ($a/t = 22$, 31, and 48) (Table A1). The cores were foamed separately in rigid molds, machined to the inside dimensions of the empty shells, and then slipped in and bonded to the shells with a minimal amount of liquid rubber. The volume of the rubber used to bond the foam to the shell was included in the analysis in a manner similar to that used for the bending specimens. These specimens showed almost no barrelling ($z_{max} < 1$ mm) (Table A3). The buckling loads of these additional specimens are represented in Figs 8(c–e), by open diamond symbols. The analysis describes their buckling loads well.

The contribution of the foam core in resisting axial compression results in a stable postbuckling regime. If serviceability is taken as the failure criterion, then the load carried by the imperfect buckled cylinder at the deflection predicted by the linear classical solution

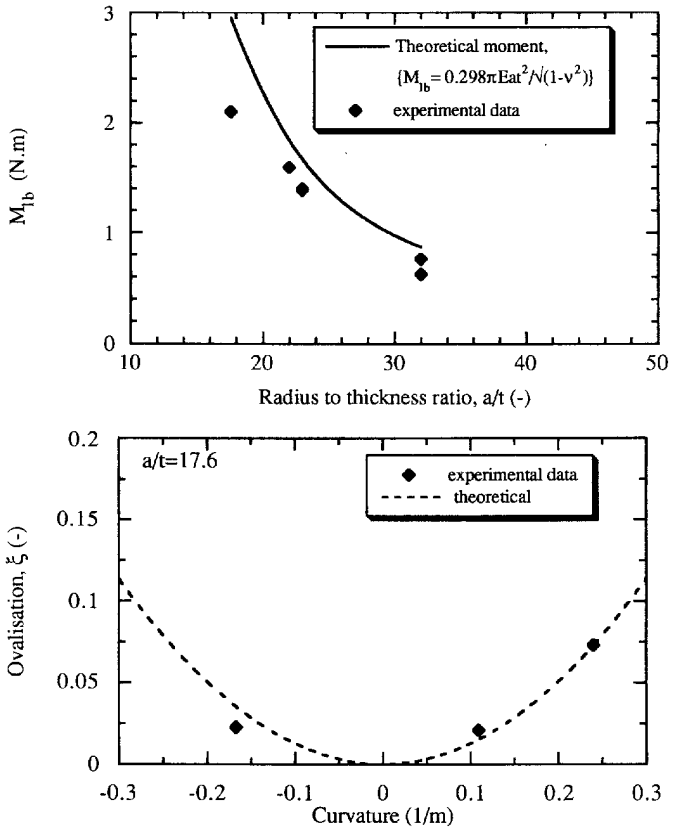

Fig. 13. (a) Local buckling moment for hollow cylinders plotted against radius to thickness ratio a/t; (b) ovalization–curvature relationship for a hollow cylinder ($a/t = 17.6$).

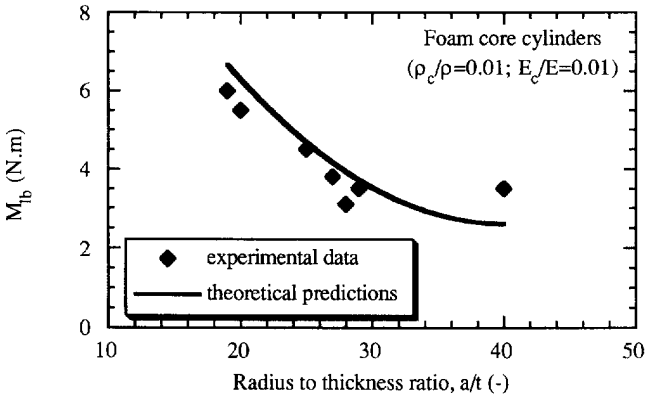

Fig. 14. Local buckling moment for partially filled cylinders plotted against radius to wall thickness ratio a/t.

should be substituted for the bifurcation load. This will result in higher failure loads for the imperfect cylinders and improved agreement with theoretical predictions.

The number of axisymmetric buckling wavelengths for the filled cylinders is plotted against a/t in Fig. 9. The solid line represents theoretical values based on the initial length of the cylinder while the dashed line takes account of the axial shortening of the cylinder in the linear elastic range before buckling occurs; there is good agreement.

The data from this study are compared with those of previous studies and with various theoretical models in Fig. 10. The new results, with the exception of the points corresponding to the most barrelled specimens with $a/t = 22$, 31, and 48, agree well with the theoretical predictions and extend the range of experimental verification by about one log cycle.

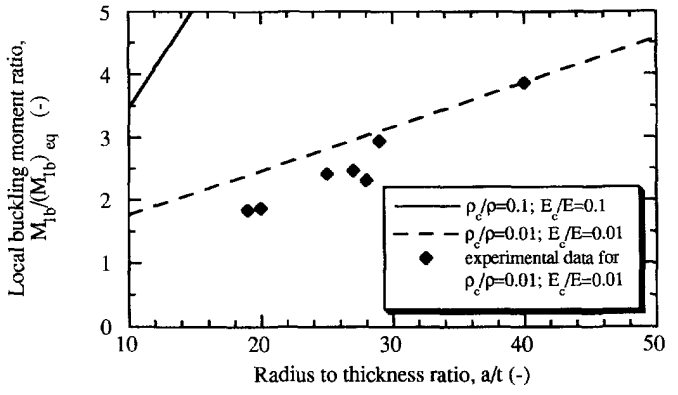

Fig. 15. Ratio of measured local buckling moment of partially filled cylinders to theoretical predictions for empty cylinders of equal weight plotted against a/t for the partially filled cylinders.

Table 3. Local buckling moments for empty and partially filled cylinders of equal weight

Mass (g)	a/t	c/t	M_{lb} experiment (Nm)	M_{lb} theory (Nm)	$M_{lb\ core}/M_{lb\ empty}$ experiment (−)	$M_{lb\ core}/M_{lb\ empty}$ theory (−)
1971	20	7	5.10	6.34	2.43	2.15
1976	17.6	—	2.10	2.95		
1566	25	8.7	4.20	4.66	3.00	2.77
1550	23	—	1.40	1.68		
1505	27	9.5	3.50	4.16	2.50	2.48
1540	23	—	1.40	1.68		
1172	40	14	3.05	2.60	4.84	2.99
1101	32	—	0.63	0.87		

Local buckling

Typical moment–curvature relationships for the four point bend specimens are presented in Fig. 12. The theoretical moment–curvature relationship can be derived from the results of the companion paper as

$$M = \pi E t a^3 C\left[\left(1+\frac{\alpha a}{4t}\left(1-\frac{b^4}{a^4}\right)+\frac{\alpha\beta' a}{8t}\right)-\frac{3}{2}\frac{a^4}{t^2}(1-\nu^2)\frac{\left(1+\frac{\alpha a}{4t}\left(1-\frac{b^4}{a^4}\right)\right)^2}{\left(1+\frac{2\alpha\beta a^3}{3t^3}(1-\nu^2)\right)}C^2\right] \quad (3)$$

with the variables defined as in the companion paper, and β and β' modified to account for the central bore hole of radius b. Note that in Fig. 12 the experimental moment curvature curves start with an offset equal to the initial conditions caused by the dead load. The experimental plots of the partially filled cylinders are linear up to about half of the theoretical critical curvature C_{cr}, and then become nonlinear, reaching a maximum. The initial linear behavior is slightly stiffer than expected due to an increase in the gripping area of the conical inserts of the bending jig as the curvature increases; this increased stiffness is most pronounced in the most compliant tubes with high a/t ratios. The last part of the plots shows a small plateau corresponding to stable local buckling which is usually followed by the localization of one buckle, the formation of an elastic hinge and the collapse of the bent cylinder [Fig. 11(b)]. In the unique case of the cylinder with $a/t = 40$, collapse did not take place and the tests were stopped when the maximum range of the x–y plotter was reached. The measured buckling wavelength was found to be between 25 and 32 mm, close to the theoretical buckling wavelength of 31 mm.

The measured local buckling moments of the hollow tubes are plotted against the radius to thickness ratio a/t in Fig. 13(a). The data lie between 70 and 95% of the theoretical

values represented by the solid line. The discrepancies are caused by the variability in the thickness of the long bending specimens. The buckling moment is proportional to the square of the thickness of the tube; some individual thickness measurements deviated from their average by up to 15%. The ovalization–curvature relationship for hollow tubes was well described by theory [eqn (12) of the previous companion paper] with stable ovalizations of up to 8% measured [Fig. 13(b)].

The local buckling moments of the silicone rubber tubes with flexible polyurethane foam cores are well described by the analysis of the previous companion paper [eqns (19) and (25)–(28)] (Fig. 14). With one exception all of the data points lie slightly below the expected values; the discrepancies are due to local imperfections and eccentricities. The buckling load for $a/t = 40$ exceeded predictions by about 15%. This is within the statistical variability of the different experimentally measured properties, especially the modulus of the rubber which showed a standard deviation of around 10%. The measured ovalizations of the partially filled four point bend tubes were found to be less than 1.5% at 80% of the critical curvatures for buckling.

Yabuta (1980) used the results of Seide (1962) for axial compression as the local buckling criterion for cylindrical shells under buckling, neglecting any ovalization or Brazier buckling. His limited data for Mylar cylinders filled with an elastic silicone rubber core are within 20% of the numerical predictions, consistent with our observation that ovalization can be neglected in a cylindrical shell with a compliant core. However, his data for hollow cylinders are less than 60% of the predicted loads as a result of neglecting the ovalization at local buckling. Accounting for ovalization ($\zeta_{lb} = 0.145$), the theoretical buckling stress is reduced to $(1 - 3\zeta_{lb}) = 56\%$ of its axial compression value, bringing the theory into good agreement with the data.

In Fig. 15 the ratios of the measured local buckling moment of the partially filled cylinders to the theoretical local buckling moment of hollow cylinders of equal weight show gains of 50–400% in strength for $a/t = 20$–50. The data points show the same increasing trend with increasing a/t that the theory predicts, falling at most to 25% below predictions. The range of a/t are characteristic of plant stems and grasses, which have a/t ratios from 10–70.

5. CONCLUSIONS

The uniaxial compression data for the buckling load, the effect of core depth and the buckling wavelength are well described by the analysis of the companion paper. The measured buckling stresses of foam filled cylinders fell along the trend compiled from the literature and have substantially extended the experimental verification range of the theoretical predictions (Fig. 10). Cylinders with foam cores showed a reduced sensitivity to imperfections caused by the manufacturing process and displayed a stable postbuckling behavior, both missing characteristics in conventional hollow shells.

The elastic buckling of both hollow and partially filled cylindrical shells in pure bending was shown to be well described by combining an axial buckling stress criterion with Brazier's ovalization analysis. The presence of a foam core reduced the ovalization at incipient local buckling from 15% for an empty tube to less than 1.5%. The measured moment–curvature relationships showed a nonlinear behavior while the analysis predicted an almost linear relationship. The discrepancy was found to be due to gripping friction and premature local buckling. The critical buckling loads and bending moments of partially filled cylinders increased by up to 400% above those of equivalent hollow cylinders, as suggested by the analysis in the companion paper.

The results suggest that biomimicking of natural cylindrical shells such as plant stems may lead to improved design of engineering cylindrical shell structures.

Acknowledgments—We are grateful to Mr. Arthur Rudolph and Mr. Steven Rudolph of the Department of Civil and Environmental Engineering, MIT, for assistance in machining and assembling the testing rigs used in the experimental program. Mr. Robert Mendoza assisted with the four point bending tests. We also wish to acknowledge the National Science Foundation (Grant Numbers MSS-9202202 and EID 9023692), which provided funding for this project.

REFERENCES

Almroth, B. O. and Brush, D. O. (1963). Postbuckling behavior of pressure- or core-stabilized cylinders under axial compression. *AIAA J.* **1**(10), 2338–2341.

Brazier, L. G. (1927). On the flexure of thin cylindrical shells and other thin sections. *Proc. R. Soc. London* **116A,** 104–114.

Cimpoeru, S. J. and Murray, N. W. (1993). The large deflection pure bending properties of a square thin-walled tube. *Int. J. Mech. Sci.* **35**(3/4), 247–256.

de Neufville, R. L. (1965). Buckling mechanism of thin cylinders under axial load. Ph.D. Thesis, Massachusetts Institute of Technology, Cambridge, MA.

Goree, W. S. and Nash, W. A. (1962). Elastic stability of circular cylindrical shells stabilized by a soft elastic core. *Exp. Mechanics* **2,** 142–149.

Gough, G. S., Elam, C. F. and deBruyne, N. A. (1940). The stabilisation of a thin sheet by a continuous supporting medium. *J. R. Aero. Soc.* **44,** 12–43.

Hutchinson, J. W. (1965a). Axial buckling of pressurized imperfect cylindrical shells. *AIAA J.* **3**(8), 1461–1466.

Hutchinson, J. W. (1965b). Buckling of imperfect cylindrical shells under axial compression and external pressure. *AIAA J.* **3**(10), 1968–1970.

Kachman, D. R. (1959). Test report on buckling of propellant cylinders under compressive loads. Space Technology Labs, Inc., GM 59-7520.6-24, 30 November.

Karam, G. N. and Gibson, L. J. (1994). Elastic buckling of cylindrical shells with elastic cores—I. Analysis. *Int. J. Solids Structures* **32,** 1259–1283.

Koiter, W. T. (1963). Elastic stability and post-buckling behavior. In *Proc. Symp. Non-Linear Problems* (Edited by R. E. Langer), pp. 257–275. University of Wisconsin Press, Madison, WI.

Kyriakides, S. and Shaw, P. K. (1982). Response and stability of elastoplastic circular pipes under combined bending and external pressure. *Int. J. Solids Structures* **18**(11), 957–973.

Kyriakides, S. and Shaw, P. K. (1987). Inelastic buckling of tubes under cyclic bending. *J. Pressure Vessel Tech.* **109,** 169–178.

Malyutin, I. S., Pilipenko, P. B., Georgievskii, V. P. and Smykov, V. I. (1980). Experimental and theoretical study of the stability in axial compression, of cylindrical shells reinforced with an elastic filler. *Prikladnaya Mekhanika* **16,** 56–60.

McIvor, I. K., Anderson, W. J. and Bijak-Zochowski, M. (1977). An experimental study of the large deformation of plastic hinges. *Int. J. Solids Structures* **13,** 53–61.

Reddy, B. D. (1979). An experimental study of the plastic buckling of circular cylinders in pure bending. *Int. J. Solids Structures* **15,** 669–683.

Rhodes, J. and Harvey, M. (1971). Alternative approach to light gage beam design. *J. Struct. Div. ASCE* **97,** 2119–2135.

Seide, P. (1962). The stability under axial compression and lateral pressure of circular cylindrical shells with a soft elastic core. *J. Aerospace Sci.* **29,** 851–862.

Sherman, D. R. (1976). Tests of circular steel tubes in bending. *J. Struct. Div. ASCE,* **102,** 2181–2195.

Sherman, D. R. (1983). Bending capacity of fabricated pipes. Report, Department of Civil Engineering, University of Wisconsin, Milwaukee, WI.

Tennyson, R. C. (1963). A note on the classical buckling of load of circular cylindrical shells under axial compression. *AIAA J.* **1**(2), 475–476.

Tennyson, R. C. (1964). Buckling of circular cylindrical shells in axial compression. *AIAA J.* **2**(7), 1351–1353.

Tennyson, R. C. (1967). *Photoelastic circular cylinders in axial compression*, STP 419. American Society for Testing and Materials, Philadelphia, PA.

Weingarten, V. I., Morgan, E. J. and Seide, P. (1965a). Elastic stability of thin-walled cylindrical and conical shells under axial compression. *AIAA J.* **3**(3), 500–505.

Weingarten, V. I., Morgan, E. J. and Seide, P. (1965b). Elastic stability of thin-walled cylindrical and conical shells under combined internal pressure and axial compression. *AIAA J.* **3**(3), 500–505.

Weingarten, V. I. and Wang, Y. S. (1976). Stability of shells attached to elastic core. *J. Engng Mech. Div., ASCE* **102,** 839–849.

Yabuta, T. (1980). Effects of elastic supports on the buckling of circular cylindrical shells under bending. *J. Appl. Mech. ASME* **47,** 866–870.

Yamaki, N. (1984). *Elastic Stability of Circular Cylindrical Shells*. North-Holland Series in Applied Mathematics and Mechanics, Elsevier Science, NY.

Yao, J. C. (1962). Buckling of axially compressed long cylindrical shell with elastic core. *J. Appl. Mech.* **29,** 329–334.

APPENDIX: DIMENSIONS AND PROPERTIES OF THE SPECIMENS USED IN THE EXPERIMENTAL PROGRAM

Table A1. Elastic moduli of the solid rubber hollow uniaxial compression specimens

Specimen designation	D (mm)	t (mm)	a/t (–)†	E (MPa)	
A2 (S 10%, nd)	113	11.80	4.3	1.97	(0.126)‡
A3 (S 10%, d)	113	11.90	4.3	2.204	(0.023)
A4 (S 10%, d)	113	11.82	4.3	2.197	(0.022)
B3 (S 10%, nd)	133	6.23	10	1.97	(0.126)
B4 (S 10%, d)	133	6.30	10	2.204	(0.023)

B5 (S 10%, d)	133	6.28	10	2.197	(0.022)
C1 (S 10%, sp)	132	2.77	22	2.197	(0.022)
C2 (FT 10%, sp)	132	2.92	22	1.412	(0.078)
C3 (F 10%, sp)	132	2.83	22	2.388	(0.144)
C4§(F 10%, sp)	132	3.02	22	2.388	(0.144)
D3 (F 10%, sp)	132	2.02	31	2.33	—
D4 (F 10%, sp)	132	2.12	31	2.388	(0.144)
D5 (F 10%, sp)	132	2.05	31	2.388	(0.144)
E1 (FT 10%, sp)	132	1.37	48	1.412	(0.078)
E2 (F 10%, sp)	132	1.26	48	2.388	(0.144)
E3 (F 10%, sp)	132	1.46	48	2.388	(0.144)
		"Quasi-perfect" specimens			
C5 (F 10%, sp)	132	2.565	22	2.110	(0.090)
D7 (F 10%, sp)	132	2.014	31	2.110	
E5 (F 10%, sp)	132	1.338	48	2.110	

In the specimen designation, S stands for slow catalyst, F for fast catalyst, FT for fast catalyst and thinner, nd, d and sp for not de-aired, de-aired and spun, respectively.

† a/t ratios are the mean values of the actual a/t ratios calculated from the outer diameter D, and the measured thicknesses t of the shell as $a/t = (D-t)/2t$, for the five size groups.

‡ The numbers in parentheses are standard deviations.

§ Cylinder C4 was kept empty.

Table A2. Elastic moduli of the solid rubber hollow four point bending specimens

Specimen designation	t (mm)	a/t (−)†	a/t_{cor} (−)‡	E (MPa)
C7 (F 10%, sp)	1.73	42	29	2.2 (0.204)
C8 (F 10%, sp)	1.32	55	40	2.2 (0.204)‖
C9 (F 10%, sp)	2.25	32	25	2.2 (0.204)‖
C11§ (F 10%, sp)	2.25	32	–	2.2 (0.204)‖
C12 (F 10%, sp)	1.83	40	28	2.2 (0.204)‖
C13 (F 10%, sp)	2.16	34	27	2.2 (0.204)‖
C15 (F 10%, sp)	3.28	22	19	2.2 (0.204)‖
C16 (F 10%, sp)	3.12	23	20	2.2 (0.204)‖
C17§ (F 10%, sp)	3.12	23	—	2.2 (0.204)‖
C18§ (F 10%, sp)	4.15	17.6	—	2.2 (0.204)‖

In the specimen designation, F stands for fast catalyst and sp for spun.

† a/t ratios are calculated from the outer diameter $D = 146$ mm and the measured thicknesses t of the shell as $a/t = (D-t)/2t$.

‡ $(a/t)_{cor}$ are the a/t ratios of the foam filled cylinders corrected to account for the additional solid rubber used to bond the foam and seal the shell.

§ Cylinders C11, C17 and C18 were kept empty.

‖ The numbers in parentheses are standard deviations.

Table A3. Maximum amplitude of profile barrelling in axially compressed cylinders with a foamed in place core

Specimen designation	Maximum barrelling amplitude (mm)	z_{max}/t (−)
A4	1.25	0.1
B5	2.0	0.3
C3	4.03	1.4
D4	4.95	2.3
D5	4.11	2.0
E1	3.68	2.7
E2	5.0	3.9
"Quasi-perfect" specimen, core not foamed in place		
C5	1.15	0.4
D7	1.65	0.8
E5	1.15	0.9